Colloquium or Thematic Topic: Fire and Explosion Safety

14th U.S. National Combustion Meeting
Organized by the Eastern States Section of the Combustion Institute
March 16–19, 2025
Boston, Massachusetts

# Module-Scale Thermal Runaway Propagation: Theory and Analysis

*Danyal Mohaddes*[1,*] *and Yi Wang*[1]

[1]*FM, Research Division, 1 Technology Way, Norwood MA, USA*
[*]*Corresponding author:* danyal.mohaddes@fmglobal.com

**Abstract:** Lithium-ion batteries (LIBs) are prevalent in consumer and industrial applications due to their high energy density and long cycle life. When abused, they can undergo thermal runaway (TR), characterized by rapid localized heating that propagates as a thermo-chemically reacting front. In Battery Energy Storage Systems (BESS), TR in one LIB can thermally abuse neighboring cells within an enclosed module, leading to a cascade of failures known as thermal runaway propagation (TRP). This work parametrically examines TRP across a LIB module in a non-dimensional formulation, focusing on pouch-format cells suitable for quasi-one-dimensional unsteady analysis. Key non-dimensional groups influencing the solution are identified from the governing equations, and the non-dimensional mean consumption rate is derived as a scalar hazard metric for the module. Numerical solutions demonstrate how this hazard metric depends on the non-dimensional groups. We identify a parameter regime where inter-cell TRP is entirely inhibited, defining a passively safe design space for LIB modules. This formulation provides designers and engineers with a formalized approach and compact parameter set to compare and mitigate TR hazards in different LIB modules.
***Keywords:*** ***Thermal runaway, Lithium-ion batteries, Fire safety***

## 1. Introduction

Battery Energy Storage Systems (BESS) stabilize power grids with high penetration of intermittent renewable energy sources [1]. In BESS, multiple LIBs are packed together in enclosed modules, assembled into racks, and housed within containers to form units of the system. While LIBs are ubiquitous due to their high energy density and long cycle life, they pose safety hazards if abused electrically, mechanically, or thermally due to thermal runaway (TR) [2]. TR is characterized by rapid localized heating from internal short circuits, self-discharge and exothermic chemical reactions, leading to a propagating thermo-chemically reacting front referred to as intra-cell thermal runaway propagation (TRP). This process generates large quantities of flammable gases, increasing internal pressure and eventually cell rupture [3]. The vented gases can ignite, posing fire and explosion hazards, and the heat generated in one cell can thermally abuse neighboring cells, initiating inter-cell TRP.

Given the widespread use of LIBs and growing importance of BESS, significant efforts have been dedicated to understanding TRP. Experimental studies have highlighted key factors such as cell chemistry, state of charge (SOC), and thermal abuse conditions in determining TR onset and vent gas characteristics [3]. Simplified stack experiments with pouch cells have demonstrated the importance of thermal boundary conditions between cells for inter-cell TRP [4]. At module and

rack scales, complexities like enclosure effects, gas flow paths and structural materials, such as plastics and metals, significantly impact TR phenomena [5].

Numerical modeling approaches have developed in tandem with experimental efforts by analyzing TRP in pouch-format LIBs at varying levels of thermal and chemical modeling complexity [6, 7]. These models achieve quantitative agreement with experiments but often require many physical and chemical input parameters, some obtained through optimization against experimental data. Recent theoretical developments have aimed to extract physical insights into TRP using thermal and combustion theory. Zhao et al. [8] derived an expression for the propagation rate of the TR front within thermally homogeneous LIB cells, showing dependencies similar to laminar flame speeds. For multi-cell stacks, Kurzawski et al. [9] analyzed heat transfer within and between cells, identifying the Biot number as a key factor controlling inter-cell TRP in unsteady settings.

In this work, we formulate TRP in an unsteady, non-dimensional context suitable for theoretical analysis. Our objective is to reduce the parameter space to key non-dimensional groups, revealing important physical sensitivities. We aim to derive a hazard metric for the system, expressed in terms of these non-dimensional parameters, providing designers and engineers with a tool to compare and potentially mitigate TR hazards in different LIB modules.

## 2. Mathematical formulation

We consider an idealized configuration of a stack of pouch-format LIB cells enclosed in a module, similar to that in Ref. [10], as shown in Fig. 1. The stack consists of $N$ cells, labeled $i = 0$ through $i = N-1$, with thermal resistance $\mathscr{R}$ between adjacent cells due to air gaps or interstitial materials. The left-most cell ($i = 0$) interfaces with an electric heater, and the right-most cell ($i = N-1$) is exposed to the ambient environment. We neglect plastic scaffolding, structural materials, and other components within the module, assuming they do not participate in the TRP process.

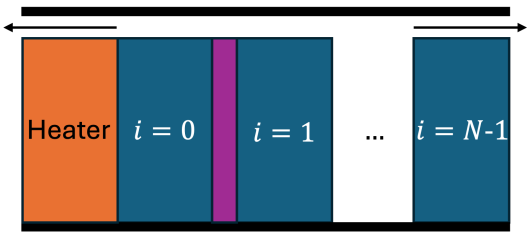


Figure 1: Schematic representation of the problem configuration. Blue rectangles indicate LIB cells numbered $i = 0$ through $i = N-1$, and the orange rectangle denotes a heater. The magenta rectangle represents the thermal resistance between LIBs, whether due to a small air gap or another material. Heavy black lines represent the module casing, and arrows indicate the vented gas paths.

### 2.1 Governing equations

Each cell, of thickness $L$, is treated as a continuum with homogeneous material properties, neglecting the many thin layers of anode, cathode and separator materials of which it is comprised, as well as the cell casing. The conservation equations for mass-specific enthalpy $h$ and species mass fractions $\vec{Y} = [Y_1, Y_2, \ldots]^T$ are

$$\partial_t(\rho h) = -\nabla\cdot\vec{\boldsymbol{q}}'' + \dot{Q}_r''' - h_v\dot{m}_v''', \quad \partial_t(\rho\vec{Y}) = -\nabla\cdot\vec{\boldsymbol{j}}'' + \vec{\dot{\omega}}''' - \vec{\dot{m}}_v''', \quad \partial_t\rho = -\dot{m}_v'''. \tag{1}$$

Here, $\rho$ is the local density, $\vec{q}''$ is the heat flux vector, $\dot{Q}_r'''$ is the internal heat generation rate, $h_v$ is the enthalpy of the ejecta, $\dot{m}_v'''$ is the total mass venting rate, $\vec{m}_v'''$ is the vector of venting rates of individual species, $\vec{j}''$ is the species diffusion flux vector, and $\vec{\omega}'''$ is the net production rate vector.

Due to the high in-plane thermal conductivity of LIBs compared to the through-thickness direction [4], we assume rapid in-plane thermal equilibration and model the problem as quasi-one-dimensional in the through-thickness direction. The spatial coordinate $x$ spans $0 \leq x \leq L$ within each cell $i$. We adopt Fourier's law for heat conduction, and decompose $-\nabla \cdot \vec{q}''$ into two components, $\partial_x(\lambda \partial_x T) + \gamma \dot{q}_e''$, where $\lambda$ is the thermal conductivity, $T$ is the local temperature, $\gamma$ is the ratio of the plane perimeter to the plane area and $\dot{q}_e''$ is the heat flux on the narrow edge of the battery. Neglecting edge heat transfer, i.e., $\gamma \dot{q}_e'' \ll \partial_x(\lambda \partial_x T)$, we focus on face heat transfer between cells. We assume negligible species diffusivity in the solid phase, i.e., $\vec{j}'' \approx \vec{0}$.

We approximate the reaction system as a single, one-step decomposition reaction obeying Arrhenius kinetics: $R \rightarrow \nu_p P + \nu_g G$, where $R$, $P$, and $G$ represent the solid reactant, solid product, and gaseous product, respectively, with mass-based stoichiometric coefficients $\nu_p$ and $\nu_g$. We assume that by mass, the solid reactant mostly produces solid product, i.e., $\nu_p \approx 1$ and $\nu_g/\nu_p \ll 1$. We further assume that gaseous mass generated is vented immediately, i.e., $\dot{\omega}_G''' = \dot{m}_{v,G}'''$, and that solid mass venting is negligible. With this, we assume that the system's mass loss is negligible relative to its initial density, i.e., $\dot{m}_v'''/\rho_0 \approx 0$ where $\rho_0$ is the initial density, These assumptions imply constant density, i.e., $\rho \approx const$. We thus simplify the governing equations, dropping the equation for $\rho$ and dropping venting terms from the energy and species equations. We also need only carry the equation for species $R$. The reaction rate becomes $\dot{\omega}_R''' = -\rho Y_R A \exp(-T_a/T)$, and the internal heat generation rate is $\dot{Q}_r''' = \Delta h_r \dot{\omega}_R'''$, where $Y_R$ is the mass fraction of $R$, $\Delta h_r$ is the heat of reaction, $A$ is the pre-exponential factor, and $T_a$ is the activation temperature. Dropping the subscript $R$ for simplicity of notation, the simplified governing equations for each cell $i$ are

$$\rho c \partial_t T_i = \lambda \partial_{xx}^2 T_i + \rho \Delta h_r Y_i A \exp(-T_a/T_i), \quad \rho \partial_t Y_i = -\rho Y_i A \exp(-T_a/T_i). \tag{2}$$

### 2.2 Propagation in an infinite-length module

We consider the case where we are not interested in the initiation behavior of the module at its extremities, but rather in the cell-to-cell propagation on the module's interior. We thus let $N \rightarrow \infty$, such that the effects of the $(i = 0, x = 0)$ and $(i = N-1, x = L)$ boundary conditions are immaterial to the dynamics of the system in the cells $0 \ll i \ll N$. For interior battery cells, the system becomes independent of the battery index, i.e, dynamics in cells $i$ and $i+1$ become identical. Assuming heat transfer between cells occurs solely via their faces, modeled with a constant thermal resistance $\mathscr{R}$, the boundary conditions for interior cells are

$$-\lambda \partial_x T_i\Big|_{x=0} = \frac{T_{i-1}(L,t) - T_i(0,t)}{\mathscr{R}}, \quad -\lambda \partial_x T_i\Big|_{x=L} = \frac{T_i(L,t) - T_{i+1}(0,t)}{\mathscr{R}}. \tag{3}$$

To formally access the reacting solution branch, we consider cell $i = 0$ to be in a 'fully reacted' state and apply our analysis away from this location, i.e.,

$$T_{i=0}(x,0) = T_b, \quad Y_{i=0}(x,0) = 0, \tag{4}$$

where $T_b = T_0 + Y_0 \Delta h_r / c$ is the solid-phase equivalent of the adiabatic flame temperature, $T_0$ is the initial temperature and $Y_0$ is the initial species mass fraction of $R$, with the balance of the initial

mass fraction being $P$. $Y_0$ is used to model the effect of state of charge [7]. For all cells $i > 0$,

$$T_i(x,0) = T_0, \quad Y_i(x,0) = Y_0. \tag{5}$$

Formally, since we initiate TR from $i = 0$ and consider rightward propagation only, the configuration is 'semi-infinite'. Semi-infinite analyses typically focus on dynamics near the finite-side boundary. The initiation condition we consider attempts to minimize the effect of the left boundary on the solution of the interior, and we will apply our analysis away from the boundary. We thus refer to the configuration as 'infinite'.

### 2.3 Non-dimensional equations

Introducing scales for variables as $\tilde{x} = L$, $\tilde{t} = \tilde{x}^2/(\lambda/\rho c)$, $\tilde{T} = T_a$, and $\tilde{Y} = Y_0$, and non-dimensionalizing each variable $\phi$ using its corresponding scale as $\phi^* = \phi/\tilde{\phi}$, we obtain

$$\partial_{t^*} T_i^* = \partial_{x^* x^*} T_i^* + QDaY_i^* \exp\left(-1/T_i^*\right), \quad \partial_{t^*} Y_i^* = -DaY_i^* \exp\left(-1/T_i^*\right) \tag{6}$$

with boundary conditions

$$-\partial_{x^*} T_i^*\Big|_{x^*=0} = Bi\left(T_{i-1}^*(1,t^*) - T_i^*(0,t^*)\right), \quad -\partial_{x^*} T_i^*\Big|_{x^*=1} = Bi\left(T_i^*(1,t^*) - T_{i+1}^*(0,t^*)\right), \tag{7}$$

and initial conditions

$$T_{i=0}^*(x^*,0) = T_b^*, \quad Y_{i=0}^*(x^*,0) = 0, \quad T_{i>0}^*(x^*,0) = T_u^*, \quad Y_{i>0}^*(x^*,0) = 1, \tag{8}$$

where we define the thermo-diffusive Damköhler number $Da = \tilde{t}/(1/A)$, non-dimensional heat of reaction $Q = \tilde{Y}\Delta h_r/(c\tilde{T})$, Biot number $Bi = (1/\mathscr{R})/(\lambda/\tilde{x})$, and initial temperature $T_u^* = T_0/\tilde{T}$, and $T_b^* = T_u^* + Q$.

#### 2.3.1 Quantity of interest

There are two questions of practical interest we seek to address, namely: (1) what is the heat generation rate in the battery due to thermal runaway, $\dot{Q}_r(t)$, and (2) assuming the vented gases burn, what is the heat generation rate due to their combustion, $\dot{Q}_c(t)$. For the former, we can simply spatially integrate the dimensional internal heat generation rate $\dot{Q}_r'''$:

$$\dot{Q}_r(t) = A_c \sum_{i=0}^{N} \int_0^L \dot{Q}_r'''(x,t)dx = A_c \Delta h_r \sum_{i=0}^{N} \int_0^L -\rho\,\partial_t Y dx, \tag{9}$$

where $A_c$ is the cell plane area. Defining a heat flux scale as $\tilde{q} = \lambda\tilde{T}/\tilde{x}$, we non-dimensionalize $\dot{Q}_r'''$ as $\dot{Q}_r^* = \dot{Q}_r/(A_c\tilde{q})$ to obtain

$$\dot{Q}_r^*(t^*) = Q \sum_{i=0}^{N} \int_0^1 -\partial_{t^*} Y^* dx^*. \tag{10}$$

Assuming complete combustion of vented gases with heat of combustion $\Delta h_c$, the heat generation rate from combustion should scale as

$$\dot{Q}_c(t) \sim A_c \nu_g \Delta h_c \sum_{i=0}^{N} \int_0^L -\rho\,\partial_t Y dx = C\dot{Q}_r(t), \tag{11}$$

where $C = \nu_g(\Delta h_c/\Delta h_r)$. Thus, $\dot{Q}_c^*(t^*) = C\dot{Q}_r^*(t^*)$. We observe that both dimensional quantities of interest, $\dot{Q}_r$ and $\dot{Q}_c$, are directly proportional to a single non-dimensional quantity, which we define as the non-dimensional consumption rate

$$\Phi^*(t^*; Da, Q, T_u^*, Bi) = \sum_{i=0}^{N} \int_0^1 -\partial_{t^*} Y^* dx^*. \tag{12}$$

In the limit of large $N$, away from the module extremities, we can assume that consumption is oscillatory but non-accelerating over multiple cells. The mean consumption rate is then

$$\bar{\Phi}^* = \frac{1}{\Delta t^*} \int_{t_0^*}^{t_0^*+\Delta t^*} \Phi^* dt^*, \tag{13}$$

where $\Delta t^*$ is sufficiently large such that the choice of $t_0^*$ is arbitrary. We note that for a propagating front with non-accelerating behavior over multiple cells, the mean consumption rate relates to the mean front propagation speed as $\bar{\Phi} = \rho A_c \bar{S}$, which after non-dimensionalization yields simply $\bar{\Phi}^* = \bar{S}^*$. We note also that in scenarios where the module is preheated, e.g., due to adjacent modules undergoing TR, the effect of elevated initial temperature can be captured by $T_u^* > 0$.

## 3. Results and discussion

For the 'infinite'-length module results shown, we choose $N = 20$. For numerical evaluation, in addition to the initiation condition on the left boundary, we require a boundary condition at the right extremity, which we set to be adiabatic. The ensuing analysis will exclusively use non-dimensional quantities, and hence we will drop the asterisks from the notation.

A solution of the governing equations of Sec. 2.3 for the parameters $[Da, Q, Bi, T_u] = [100, 1, 1, 0]$ is shown in Fig. 2. The parameters $Da$ and $Q$ were chosen to be qualitatively representative of a pouch-format LIB with a relatively slow rate of reaction and high heat of reaction, $Bi$ was chosen to be qualitatively representative of a realistic module with finite inter-cell thermal resistance, and $T_u$ was chosen to be qualitatively representative of a LIB with a large activation temperature at room temperature conditions.

The color contours in Fig. 2 show the evolution of the spatially one-dimensional system across time. For this choice of parameters, it is clear from the figure that there are both inter- and intra-cell TRP dynamics at play. The reaction zone, where the local consumption rate $-\partial_t Y \gg 0$, is thin in both space and time. A constant average propagation speed is also clearly visible despite significant local dynamics. Dynamics are identical in cells away from $i = 0$ and $i = N-1$, as intended for the present propagation analysis. The line plot in Fig. 2 shows the corresponding value of $\Phi$ over time. Considering the unsteady behavior of $\Phi$ in cells away from $i = 0$ and $i = N-1$, we find that $0.9 < \Phi < 7.9$ and $\bar{\Phi} = 3.7$. The figure demonstrates that in the limit of large $N$, the system is oscillatory but non-accelerating, i.e., in a periodic steady state, as was assumed when defining $\bar{\Phi}$.

To consider intra- and inter-cell TRP more closely, Fig. 3 shows the data of Fig. 2 focused on the behavior of two medial cells, $i = 10$ and $i = 11$, where propagation is in a periodic steady state and the dynamics of each cell are identical. Intra-cell TRP, i.e., the 'cell cross time', $\Delta t_{cct}$, is determined by the propagation speed through the local temperature-species profile. In the figure, the red line shows the front's evolution using the spatial variation of the time at which the maximum consumption rate occurs, $t_{max}(x) = \arg\max_t(-\partial_t Y)$. The slope of the red line is thus the inverse

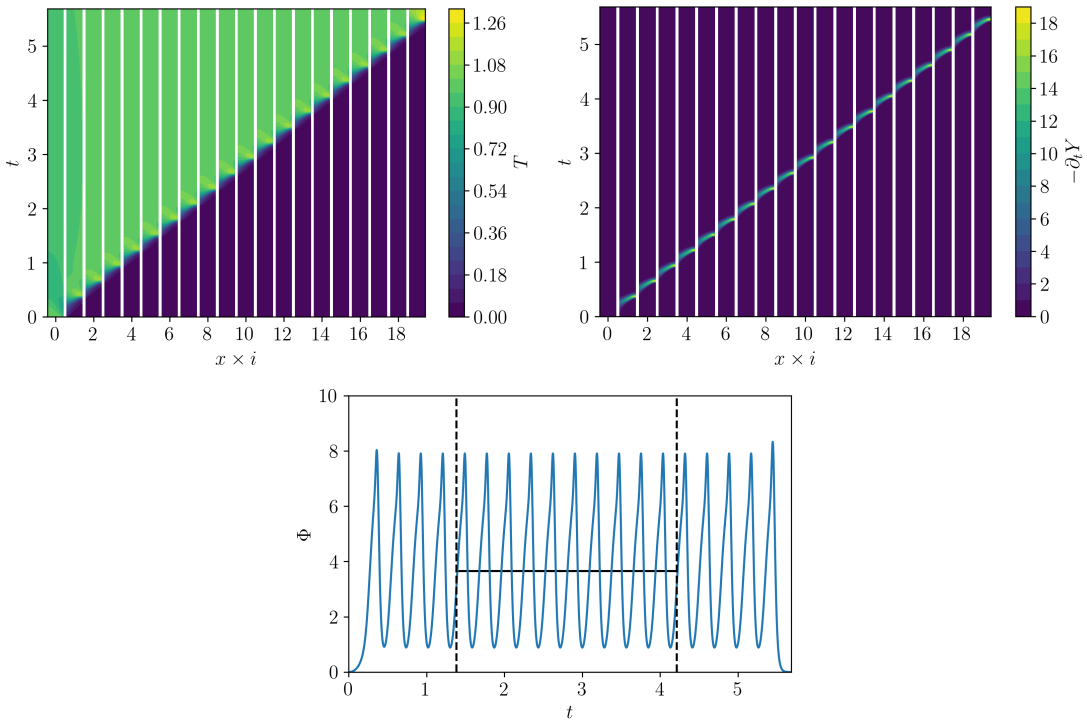


Figure 2: Top figures: space-time solution of governing equations of Sec. 2.3 with parameters $[Da, Q, Bi, T_u] = [100, 1, 1, 0]$. White vertical lines indicate boundaries between cells. Bottom figure: corresponding consumption rate. Blue line: instantaneous value, black solid line: mean value ($\bar{\Phi} = 3.7$), averaged over the middle two quarters of the unsteady solution time, i.e., between the vertical dashed black lines.

of the local propagation speed: a flatter line indicates locally faster front propagation. As seen in Fig. 3, $\Delta t_{cct}$ corresponds to the time for the front to propagate from one cell boundary to the other. Inter-cell TRP, i.e., the 'gap cross time', $\Delta t_{gct}$ corresponds to the time between the burnout of the front reaching the left inter-cell boundary and its initiation on the right. It is the analogous to a hot surface ignition delay time, where the hot surface is the left boundary of each battery cell. The thickness of the front is shown in Fig. 3 using the $Y = 0.99$ and $Y = 0.01$ isocontours.

We begin our parametric investigation of the behavior of the governing equations of Sec. 2.3 by varying $Bi$. Since this parameter controls the relative strengths of inter- and intra-cell heat transfer, it is clear that this parameter will affect the intra- and inter-cell TRP rates. Figure 4 shows results focused on two medial cells and compares behavior across $Bi$. Corresponding plots of the instantaneous consumption rate are shown in Fig. 5. We find that for $Bi \ll 1$, which might correspond to the addition of an insulating layer between cells, reaction in cell $i+1$ is temporally segregated from cell $i$, such that $\Phi = 0$ during $\Delta t_{gct}$. When $Bi \gtrsim 1$, i.e., when intra-cell thermal resistance begins to dominate inter-cell thermal resistance, reaction can begin in cell $i+1$ prior to its completion in cell $i$, such that $\Phi > 0 \forall t$. As $Bi \to \infty$, the system behavior approaches that of a single, infinitely large battery cell. In this limit, $\Phi \to \bar{\Phi} = const$ and $\Delta t_{gct} \to 0$. We see that $Bi = 10$ is already approaching this limit.

Considering the initiation and propagation behavior within medial cells in more detail, we plot $-\partial_t Y$ over space and time for different values of $Bi$ in Fig. 6. We see that for $Bi \ll 1$, cell $i-1$

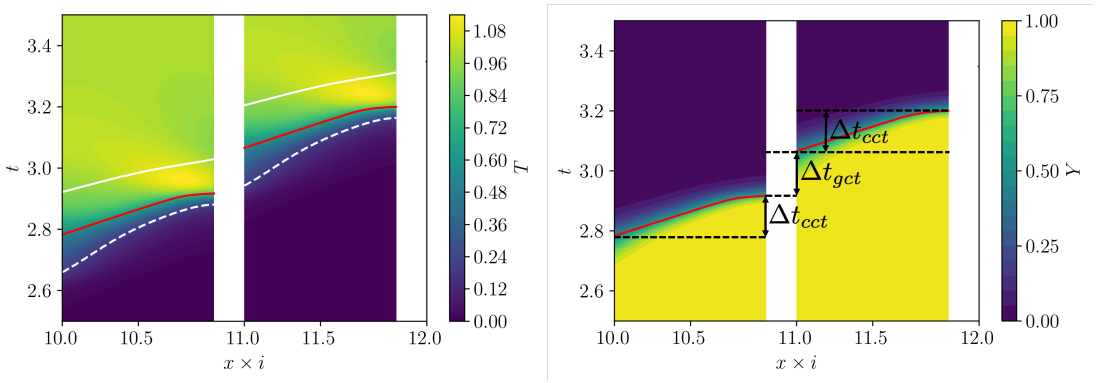


Figure 3: Results of Fig. 2 focused on two medial cells, showing $T$ and $Y$. The red line denotes the spatial variation of the time at which the maximum consumption rate occurs, $t_{max}(x) = \arg\max_t(-\partial_t Y)$. The solid and dashed white lines denote the $Y = 0.01$, $Y = 0.99$ isocontours, respectively.

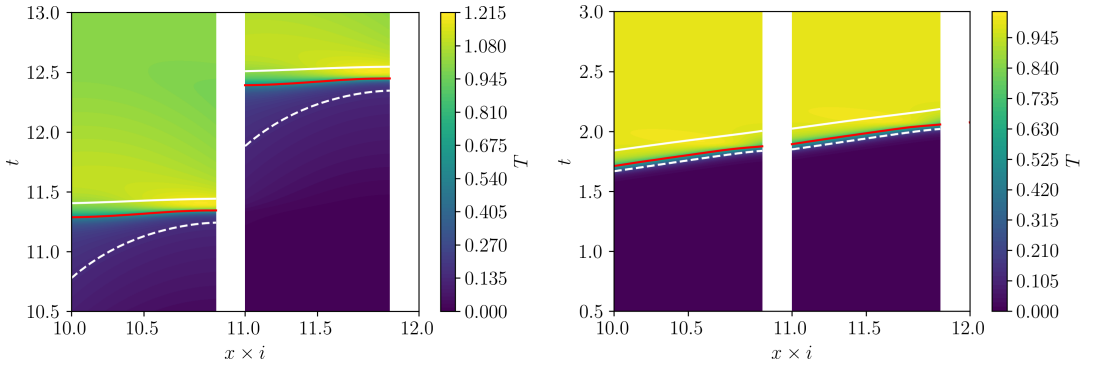


Figure 4: Results with $[Da, Q, T_u] = [100, 1, 0]$ for $Bi = 0.15$ (left) and $Bi = 10.0$ (right) focused on two medial cells ($i = 10$ and $i = 11$). The red line denotes the spatial variation of the time at which the maximum consumption rate occurs, $t_{max}(x) = \arg\max_t(-\partial_t Y)$. The solid and dashed white lines denote the $Y = 0.01$, $Y = 0.99$ isocontours, respectively.

preheats cell $i$, such that once initiation occurs, propagation starts out fast near the left boundary and slows down with $x$, then accelerates as the right boundary is approached. When $Bi \sim 1$, as was shown by the red line in Fig. 3, we observe negligible preheating from cell $i-1$, such that the propagation speed is constant from initiation until the right boundary is approached. For $Bi \lesssim 1$, we find that propagation is locally fastest and $-\partial_t Y$ greatest near the right boundary during burnout: the right boundary behaves more adiabatically for small $Bi$, and the reduced heat loss to the boundary accelerates the propagating front. As $Bi \to \infty$, initiation and burnout effects are eliminated since the system approaches the behavior of a single cell, yielding a constant propagation speed.

Having considered the spatio-temporal dynamics of the system, we now consider the effects of parametric variations on the quantity of interest, $\bar{\Phi} = \bar{\Phi}(Da, Q, Bi, T_u)$. In Figs. 7 and 8, we analyze $\bar{\Phi}$ in parameter space. We can first observe that increasing $Da$, which might correspond to a reduction in battery thermal conductivity or a more reactive battery chemistry, increases $\bar{\Phi}$, since $Da$ controls the reaction rate and thus directly couples with the consumption rate. Increasing $Q$, which might correspond to a more energetic battery composition or a higher SOC, also increases

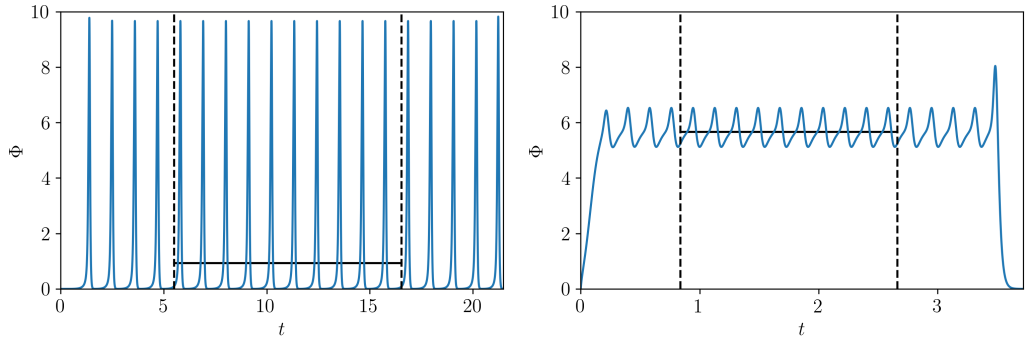


Figure 5: Instantaneous and average consumption rates over time corresponding to the results shown in Fig. 4. Left: $Bi = 0.15$, $\bar{\Phi} = 0.94$, right: $Bi = 10.0$, $\bar{\Phi} = 5.7$.

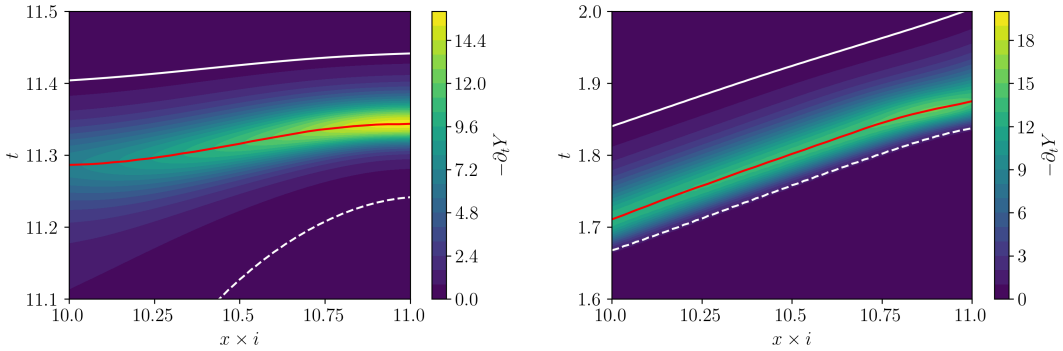


Figure 6: Results with $[Da, Q, T_u] = [100, 1, 0]$ for $Bi = 0.15$ (left) and $Bi = 10.0$ (right) focused on one medial cell ($i = 10$). The red line denotes the spatial variation of the time at which the maximum consumption rate occurs, $t_{max}(x) = \arg\max_t(-\partial_t Y)$. The solid and dashed white lines denote the $Y = 0.01$, $Y = 0.99$ isocontours, respectively.

$\bar{\Phi}$, since $Q$ controls the internal heat generation rate per unit of reacted species, thereby affecting the consumption rate through the temperature-dependent reaction rate. These two observations are as expected: faster, more exothermic chemistry yields a greater $\bar{\Phi}$.

The figures also show that increasing $Bi$ increases $\bar{\Phi}$, as was also observed in the context of Figs. 4 to 6. It suggests that increasing the inter-battery thermal resistance $\mathscr{R}$ (and thereby decreasing $Bi$) monotonically decreases $\bar{\Phi}$. Thus, although it was shown in Fig. 6 that low values of $Bi$ yield rapid propagation rates near the hot left surface due to the cell-to-cell preheating effect during the 'gap cross time', ultimately, the presence of the inter-cell thermal resistance slows the mean propagation rate, and correspondingly the mean consumption rate $\bar{\Phi}$.

Of particular interest for system safety is the observation from the figures that below a critical non-dimensional parameter combination, $\bar{\Phi} = 0$. This corresponds to situations where cell-to-cell propagation fails, i.e., the reaction is too slow and too weak to overcome the inter-cell resistance. In this regime, the system is passively safe from inter-cell TRP: were a cell to go to TR, the inter-cell cascade would eventually stop without any external intervention, rather than propagate indefinitely. Considering Fig. 8, we find that when $T_u > 0$ the conditions for which such passive safety can be achieved become more restricted, requiring either weaker chemistry (smaller $Da$ and $Q$) or greater inter-cell resistance (smaller $Bi$). This suggests that operating temperature and

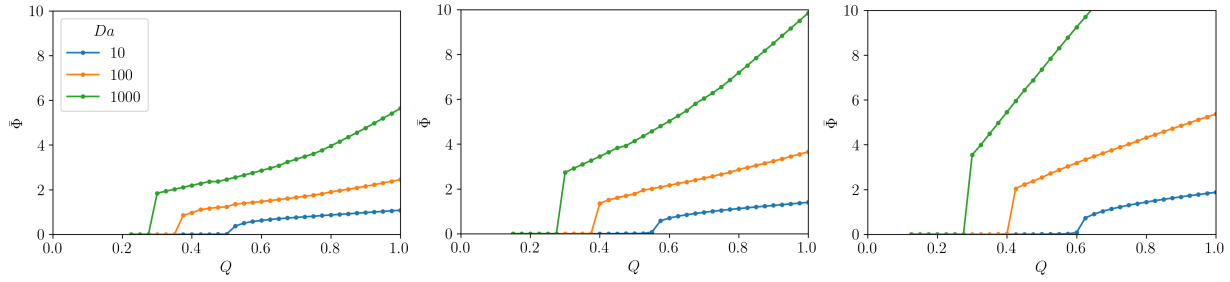


Figure 7: Parametric variation of $\bar{\Phi}$ with $T_u = 0.0$. Left: $Bi = 0.5$, middle: $Bi = 1.0$, right: $Bi = 5.0$.

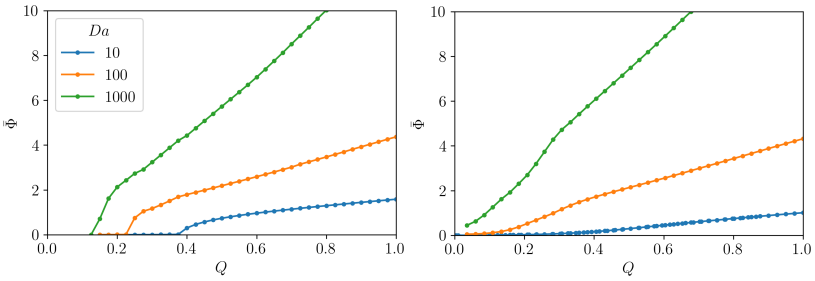


Figure 8: Parametric variation of $\bar{\Phi}$ with $Bi = 1.0$. Left: $T_u = 0.05$, right: $T_u = 0.1$.

slow heating from ambient sources, such as a neighboring module in TR, can have important effects on system safety, with the potential to make a system that is passively safe at one operating temperature capable of supporting inter-cell TRP at a higher operating temperature. These results are in agreement with the approach investigated in Ref. [9] to inhibit inter-cell TRP using an inter-cell thermal resistance, and are related to the discussion of a minimum heat flux for intra-cell TRP in a prismatic cell in Ref. [11]. Indeed, since inter-cell TRP is analogous to the problem of hot surface ignition, the existence of a regime in which propagation does not occur is qualitatively similar to the classical result for the ignition of a premixed combustible [12]: below a critical condition, heat input dissipates and does not result in a thermal explosion.

## 4. Conclusions

We developed a one-dimensional formulation in a non-dimensional setting describing the propagation of thermal runaway within and between pouch-format lithium-ion battery cells. To support our non-dimensional analysis, we employed single-step global chemistry and assumed constant physical properties. We derived a non-dimensional quantity, the mass consumption rate $\Phi$, which we showed is proportional to both the internal heat generation rate from TRP and the heat release rate of a vent gas-fueled fire. The mean consumption rate, $\bar{\Phi}$, was derived as a hazard metric dependent on four non-dimensional parameters: the thermo-diffusive Damköhler number $Da$, non-dimensional heat of reaction $Q$, Biot number $Bi$ and non-dimensional initial temperature $T_u$. Cell cross time and gap cross time were found to be outcomes of the choice of these parameters. We showed that there exists a regime in the parameter space where the module is passively safe, i.e., it does not allow for inter-cell TRP. This work provides an analytical framework within which questions regarding module safety can be explored, and inherent trade-offs between different physical quantities can be seen in a non-dimensional setting, thus supporting experiments, more detailed numerical simulations, and analyses of module designs.

**Acknowledgements**

The authors acknowledge the invaluable insights provided by the experimental scientists at FM Research, Drs. Dong Zeng, Gang Xiong, Juan Cuevas and Mr. Wilson Brown, as well as Dr. Robert Barlow of Barlow Combustion Research.

**References**

[1] Y. Yang, S. Bremner, C. Menictas, and M. Kay, Modelling and optimal energy management for battery energy storage systems in renewable energy systems: A review, Renew. Sust. Energ. Rev. 167 (2022) 112671.

[2] Q. Wang, B. Mao, S. I. Stoliarov, and J. Sun, A review of lithium ion battery failure mechanisms and fire prevention strategies, Prog. Energ. Combust. 73 (2019) 95–131.

[3] L. Gagnon, D. Zeng, B. Ditch, and Y. Wang, Cell-level thermal runaway behavior of large-format Li-ion pouch cells, Fire Safety J. 140 (2023) 103904.

[4] R. W. Kennedy and O. A. Ezekoye, Experimental and modeling characterization of nickel manganese cobalt (532) lithium ion battery arrays with thermal separators, J. Energ. Storage 60 (2023) 106682.

[5] B. Ditch and D. Zeng, Fire hazard of lithium-ion battery energy storage systems: 1. Module to rack-scale fire tests, Fire Technol. 59 (2023) 3049–3075.

[6] A. Kurzawski, L. Torres-Castro, R. Shurtz, J. Lamb, and J. C. Hewson, Predicting cell-to-cell failure propagation and limits of propagation in lithium-ion cell stacks, Proc. Combust. Inst. 38 (2021) 4737–4745.

[7] D. Zeng, D. Mohaddes, L. Gagnon, and Y. Wang, Modeling initiation and propagation of thermal runaway in pouch Li-ion battery cells: Effects of heating rate and state-of-charge, Proc. Combust. Inst. 40 (2024) 105316.

[8] P. Zhao and S. Yang, On planar reaction front in condensed materials: Reduced model, propagation speed, reaction zone balance, and insights into battery thermal runaway, Combust. Flame 245 (2022) 112346.

[9] A. Kurzawski and J. C. Hewson, Avoiding cascading failure in battery packs through thermal analysis, 13th U.S. National Combustion Meeting (2022).

[10] D. Zeng, L. Gagnon, and Y. Wang, Experimental and modeling study of thermal runaway propagation in a commercial lithium-ion battery module, 14th U.S. National Combustion Meeting (2024).

[11] L. Zhang, P. Zhao, M. Xu, and X. Wang, Computational identification of the safety regime of Li-ion battery thermal runaway, Appl. Energ. 261 (2020) 114440.

[12] Y. Zeldovich, G. Barenblatt, V. Librovich, and G. Makhviladze, The Mathematical Theory of Combustion and Explosions, Consultants Bureau, 1985.